Journal of Scientific Computing (2022) 92:31
https://doi.org/10.1007/s10915-022-01872-1

A Positivity Preserving, Energy Stable Finite Difference Scheme for the Flory-Huggins-Cahn-Hilliard-Navier-Stokes System

Wenbin Chen[1] · Jianyu Jing[2] · Cheng Wang[3] · Xiaoming Wang[4]

Received: 21 September 2021 / Revised: 20 February 2022 / Accepted: 1 April 2022

Abstract
In this paper, we propose and analyze a finite difference numerical scheme for the Cahn-Hilliard-Navier-Stokes system, with logarithmic Flory-Huggins energy potential. In the numerical approximation to the singular chemical potential, the logarithmic term and the surface diffusion term are implicitly updated, while an explicit computation is applied to the concave expansive term. Moreover, the convective term in the phase field evolutionary equation is approximated in a semi-implicit manner. Similarly, the fluid momentum equation is computed by a semi-implicit algorithm: implicit treatment for the kinematic diffusion term, explicit update for the pressure gradient, combined with semi-implicit approximations to the fluid convection and the phase field coupled term, respectively. Such a semi-implicit method gives an intermediate velocity field. Subsequently, a Helmholtz projection into the divergence-free vector field yields the velocity vector and the pressure variable at the next time step. This approach decouples the Stokes solver, which in turn drastically improves the numerical efficiency. The positivity-preserving property and the unique solvability of the proposed numerical scheme is theoretically justified, i.e., the phase variable is always between -1 and 1, following the singular nature of the logarithmic term as the phase variable

✉ Cheng Wang
cwang1@umassd.edu

Wenbin Chen
wbchen@fudan.edu.cn

Jianyu Jing
20110180021@fudan.edu.cn

Xiaoming Wang
wangxm@sustech.edu.cn

1 Shanghai Key Laboratory for Contemporary Applied Mathematics, School of Mathematical Sciences, Fudan University, 200433 Shanghai, China

2 School of Mathematical Sciences, Fudan University, 200433 Shanghai, China

3 Mathematics Department, University of Massachusetts, North Dartmouth, MA 02747, USA

4 International Center for Mathematics and Department of Mathematics, and Guangdong Provincial Key Laboratory of Computational Science and Material Design, and National Center for Applied Mathematics Shenzhen, Southern University of Science and Technology, 518055 Shenzhen, China

Published online: 18 June 2022

approaches the singular limit values. In addition, an iteration construction technique is applied in the positivity-preserving and unique solvability analysis, motivated by the non-symmetric nature of the fluid convection term. The energy stability of the proposed numerical scheme could be derived by a careful estimate. A few numerical results are presented to validate the robustness of the proposed numerical scheme.

Keywords Cahn-Hilliard-Navier-Stokes system · Flory Huggins energy potential · Positivity preserving · Monotonicity analysis · Energy stability · Numerical accuracy

Mathematics Subject Classification 35K35 · 35K55 · 49J40 · 65M06 · 65M12

1 Introduction

Let $\Omega \subset \mathbb{R}^d$ ($d = 2$ or $d = 3$) be a bounded domain. For any $\phi \in H^1(\Omega)$, with a point-wise bound, $-1 < \phi < 1$, the Flory-Huggins energy functional is given by

$$E(\phi) = \int_\Omega \left((1+\phi)\ln(1+\phi) + (1-\phi)\ln(1-\phi) - \frac{\theta_0}{2}\phi^2 + \frac{\varepsilon^2}{2}|\nabla\phi|^2 \right) d\mathbf{x}, \quad (1.1)$$

in which ε, θ_0 are positive constants associated with the diffuse interface width and inverse temperature. See the related references [2, 9, 11, 18]. In this article, we assume that $\Omega = (0,1)^3$, and consider periodic boundary conditions, for simplicity of presentation. An extension of our results for the model with homogeneous Neumann boundary conditions is straightforward.

In addition, the phase field model coupled with fluid motion has also attracted a great deal of attentions. For example, the Cahn-Hilliard-Navier-Stokes (CHNS) system is formulated as

$$\mathbf{u}_t + \mathbf{u}\cdot\nabla\mathbf{u} + \nabla p - \nu\Delta\mathbf{u} = -\gamma\phi\nabla\mu, \quad (1.2)$$

$$\phi_t + \nabla\cdot(\phi\mathbf{u}) = \Delta\mu, \quad \mu := \delta_\phi E = \ln(1+\phi) - \ln(1-\phi) - \theta_0\phi - \varepsilon^2\Delta\phi, \quad (1.3)$$

$$\nabla\cdot\mathbf{u} = 0. \quad (1.4)$$

where $\gamma > 0$ is related to surface tension, p is a pressure, the term $-\gamma\phi\nabla\mu$ is a diffuse interface approximation of the singular surface force, $\mathbf{u}$ is the advective velocity, and ν stands for the kinematic viscosity. For simplicity, we assume a constant density, i.e., $\rho \equiv 1$. The non-constant density system can be analyzed analogously. For such a system, the following energy dissipation law could be carefully derived:

$$E'_{total}(t) = -\int_\Omega |\nabla\mu|^2 d\mathbf{x} - \frac{\nu}{\gamma}\int_\Omega |\nabla\mathbf{u}|^2 d\mathbf{x} \le 0, \quad E_{total} = E(\phi) + \frac{1}{2\gamma}\|\mathbf{u}\|^2. \quad (1.5)$$

See the detailed description of the CHNS model in [34] and many related numerical works [3, 4, 6, 22, 23, 29, 30, 39, 40, 45, 50, 51] for various Cahn-Hilliard-Fluid systems, etc.

The energy stability has always been one focus issue for any numerical approximation to the CHNS system, and there have been quite a few existing works on this analysis [10, 26, 46]. Meanwhile, most existing energy stable numerical works have been based on the polynomial approximation in the energy potential, so that a singularity (as the phase variables approach the singular limit values) has been avoided. For the Flory-Huggins energy potential (1.1) and the corresponding CHNS system (1.2)–(1.4), designing a numerical scheme to preserve both the point-wise positivity (of the logarithmic arguments) and the energy stability turns

out to be very challenging, due to the highly nonlinear, singular and coupled nature of the PDE system. In this paper, we propose and analyze a numerical scheme for the CHNS system (1.2)–(1.4), with three theoretical properties justified: positivity-preserving, unique solvability, and unconditional energy stability.

The numerical approximation to the chemical potential is based on the convex-concave decomposition of the Flory-Huggins energy functional. An implicit treatment of the nonlinear singular logarithmic term is applied to theoretically justify its positivity-preserving property, while a related analysis for the explicit treatment has also been available in a recent work [31], based on the separation estimate of the gradient flow. In more details, the singular and convex nature of the logarithmic term prevents the numerical solution reach the singular limit values, so that a point-wise positivity is preserved for the logarithmic argument variables. The linear expansive term is explicitly updated, for the sake of unique solvability, due to the negative eigenvalues involved. The surface diffusion term is implicitly treated, which comes from its convexity. Such a convex splitting approach has been reported in [7] for the pure phase field model. Meanwhile, the other parts of the CHNS have to be handled very carefully, to ensure the desired theoretical properties. The convective term in the phase field dynamic equation is discretized in a semi-implicit way: explicit treatment for the phase variable and implicit treatment for the velocity vector. The fluid momentum equation is computed by a similar semi-implicit algorithm: implicit treatment for the kinematic diffusion term, explicit update for the pressure gradient, along with semi-implicit approximations to the fluid convection and the phase field coupled term, respectively. In turn, an intermediate velocity field is determined by this semi-implicit method, which could be represented as a linear velocity solver, with a fixed chemical potential profile. Subsequently, a Helmholtz projection into the divergence-free vector field yields the velocity vector and the pressure variable at the next time step. This approach decouples the Stokes solver, which in turn drastically improves the numerical efficiency. Also see an earlier work [24] of a decoupled method for incompressible fluid, and its extension to the phase-field-fluid system [35, 52], while the later ones are more focused on the polynomial approximation in the phase field energy potential, instead of the singular logarithmic ones.

The unique solvability and positivity-preserving analysis for the proposed numerical scheme turns out to be highly non-standard, due to the nonlinear, singular and coupled nature. In fact, the whole numerical system does not have a symmetric Jacobian matrix, which comes from the non-symmetric nature of the fluid convective term in the momentum equation. As a result, this numerical system could not be represented as a minimization of a given discrete energy functional, and many associated mathematical techniques are not applicable any more. And also, the singular nature in the chemical potential (as the phase variable approaches the singular limit value) prevents a direct application of the Browder–Minty lemma [1, 41], which has been a very powerful tool to deal with nonlinear, monotone, while non-symmetric systems. To overcome these subtle difficulties, we come up with a new approach to establish the unique solvability and positivity-preserving analysis. First, given a fixed chemical potential profile, the velocity vector turns out to be a linear operator on this profile. In more details, such a linear operator is non-symmetric, while a monotonicity property is valid. Subsequently, a substitution of this linear velocity operator into the phase variable evolutionary equation reveals that, the chemical potential field turns out to be another linear operator of the discrete temporal derivative of the phase variable. Furthermore, careful estimates imply the monotonicity property of this chemical potential operator, and the discrete ℓ^2 and ℓ^∞ bounds of this operator could be appropriately established. With all these preliminary estimates at hand, the whole numerical system could be represented as this chemical potential operator, combined with the original chemical potential expansion (1.3)

(including the singular logarithmic parts, the linear expansive part, and the surface diffusion term). Again, this rewritten numerical system is highly nonlinear, singular and coupled, and there is no existing theory to ensure its unique solvability. To avoid this difficulty, we propose a nonlinear iteration process in the construction of the numerical solution. In more details, the linear operator (associated with the chemical potential) is treated as the given source, corresponding to the iterate at the previous stage, while the nonlinear chemical potential expansion is applied to the iterate at the next stage, combined with a relaxation algorithm. By the nonlinear analysis presented in a recent work [7], it is known that such an iteration process creates a unique solution satisfying the positivity-preserving property at each iteration stage, which comes from the convex nature of the logarithmic terms. Moreover, the monotonicity analysis for the linear operator (associated with the chemical potential) leads to a contraction mapping estimate of this nonlinear iteration, provided that the relaxation parameter is sufficiently large. Therefore, a fixed point argument could be effectively applied, the unique solvability and positivity-preserving analysis could be theoretically justified for the proposed numerical scheme.

The energy stability of the numerical scheme is a direct consequence of a careful energy estimate, which gives a dissipation law for the discrete energy functional. The summation by parts formulas for different physical variables, combined with the staggered location of the fluid velocity vector and the phase variable, will play an important role in the analysis.

The rest of the article is organized as follows. In Sect. 2 we review the finite difference approximation over the staggered grid, and propose the numerical scheme. The detailed proof for the positivity-preserving property is provided in Sect. 3, and the modified energy stability is proved in Sect. 4. Some numerical results are presented in Sect. 5. Finally, concluding remarks are given in Sect. 6.

2 The Numerical Scheme

2.1 The Finite Difference Spatial Discretization

For simplicity of presentation, we focus our discussions on the two-dimensional (2-D) case, with the computational domain given by $\Omega = (0, 1)^2$. An extension to the three-dimensional (3-D) case is straightforward, and the details are left to the interested readers.

It is assumed that N is a positive integer such that $h = \frac{1}{N}$, which is called the spatial step size. The phase variable ϕ, as well as the chemical potential μ and and pressure field p, are evaluated at the cell-centered mesh points: $((i + 1/2)h, (j + 1/2)h)$, at the component-wise level. In turn, the discrete gradient of ϕ is evaluated at the mesh points $(ih, (j + 1/2)h)$, $((i + 1/2)h, jh)$, respectively:

$$
\begin{aligned}
(D_x\phi)_{i,j+1/2} &= \frac{\phi_{i+1/2,j+1/2} - \phi_{i-1/2,j+1/2}}{h}, \\
(D_y\phi)_{i+1/2,j} &= \frac{\phi_{i+1/2,j+1/2} - \phi_{i+1/2,j-1/2}}{h}.
\end{aligned} \tag{2.1}
$$

The five-point Laplacian takes a standard form. Similarly, the wide-stencil differences for cell centered functions could be introduced as

$$
\begin{aligned}
(\tilde{D}_x\phi)_{i+1/2,j+1/2} &= \frac{\phi_{i+3/2,j+1/2} - \phi_{i-1/2,j+1/2}}{2h}, \\
(\tilde{D}_y\phi)_{i+1/2,j+1/2} &= \frac{\phi_{i+1/2,j+3/2} - \phi_{i+1/2,j-1/2}}{2h}.
\end{aligned} \tag{2.2}
$$

Meanwhile, in order to enforce the divergence-free property of the velocity vector at the discrete level, we choose a staggered grid for the velocity field, in which the individual components of a given velocity, say, $\boldsymbol{v} = (v^x, v^y)$, are defined at the east-west cell edge points $(ih, (j + 1/2)h)$, and the north-south cell edge points $((i + 1/2)h, jh)$, respectively. This staggered grid is also known as the marker and cell (MAC) grid and was first proposed in [28] to deal with the incompressible Navier-Stokes equations, and the detailed analyses have been provided in [17, 47]. Also see the related applications to the primitive equations [43] and planetary geostrophic equations [44], *et cetera*. In addition, the discrete periodic function space is denoted as $\mathcal{C}_{\text{per}}$, for all the physical variables, located at the corresponding mesh points.

The discrete divergence of $\boldsymbol{v}$, specifically,

$$\nabla_h \cdot \boldsymbol{v} = D_x v^x + D_y v^y,$$

is defined at the cell center points $((i + 1/2)h, (j + 1/2)h)$ as follows:

$$(\nabla_h \cdot \boldsymbol{v})_{i+1/2,\, j+1/2} := \left(D_x v^x\right)_{i+1/2,\, j+1/2} + \left(D_y v^y\right)_{i+1/2,\, j+1/2}.$$

One key advantage of the MAC grid approach is that the discrete divergence of the unknown grid velocity will always be identically zero at every cell center point. Such a divergence-free property at the discrete level comes from the special structure of the MAC grid and assures that the velocity field is orthogonal to a corresponding discrete pressure gradient at the discrete level; see also reference [17].

For $\boldsymbol{u} = (u^x, u^y)^T$, $\boldsymbol{v} = (v^x, v^y)^T$, located at the staggered mesh points $(x_i, y_{j+1/2})$, $(x_{i+1/2}, y_j)$, respectively, and the cell centered variables ϕ, μ, the following terms are evaluated as

$$\boldsymbol{u} \cdot \nabla_h \boldsymbol{v} = \begin{pmatrix} u^x_{i,j+1/2} \tilde{D}_x v^x_{i,j+1/2} + \mathcal{A}_{xy} u^y_{i,j+1/2} \tilde{D}_y v^x_{i,j+1/2} \\ \mathcal{A}_{xy} u^x_{i+1/2,j} \tilde{D}_x v^y_{i+1/2,j} + u^y_{i,j+1/2} \tilde{D}_y v^y_{i+1/2,j} \end{pmatrix}, \tag{2.3}$$

$$\nabla_h \cdot (\boldsymbol{v}\boldsymbol{u}^T) = \begin{pmatrix} \tilde{D}_x (u^x v^x)_{i,j+1/2} + \tilde{D}_y (\mathcal{A}_{xy} u^y v^x)_{i,j+1/2} \\ \tilde{D}_x (\mathcal{A}_{xy} u^x v^y)_{i+1/2,j} + \tilde{D}_y (u^y v^y)_{i+1/2,j} \end{pmatrix}, \tag{2.4}$$

$$\mathcal{A}_h \phi \nabla_h \mu = \begin{pmatrix} (D_x \mu \cdot \mathcal{A}_x \phi)_{i,j+1/2)i,j+1/2} \\ (D_y \mu \cdot \mathcal{A}_y \phi)_{i+1/2,j)i+1/2,j} \end{pmatrix}, \tag{2.5}$$

$$\nabla_h \cdot (\mathcal{A}_h \phi \boldsymbol{u}) = D_x (u^x \mathcal{A}_x \phi)_{i+1/2,j+1/2} + D_y (u^y \mathcal{A}_y \phi)_{i+1/2,j+1/2}, \tag{2.6}$$

where the following averaging operators have been employed:

$$\mathcal{A}_{xy} u^x_{i+1/2,j} = \frac{1}{4} \left(u^x_{i,j-1/2} + u^x_{i,j+1/2} + u^x_{i+1,j-1/2} + u^x_{i+1,j+1/2} \right), \tag{2.7}$$

$$\mathcal{A}_x \phi_{i,j+1/2} = \frac{1}{2} \left(\phi_{i-1/2,j+1/2} + \phi_{i+1/2,j+1/2} \right). \tag{2.8}$$

A few other average terms, such as $\mathcal{A}_{xy} u^y_{i,j+1/2}$, $\mathcal{A}_y \phi_{i+1/2,j}$, could be defined in the same manner.

Definition 2.1 For any pair of variables u^a, u^b which are evaluated at the mesh points $(i, j + 1/2)$, (such as u, $D_x \phi$, $D_x \mu$, $D_x p$, *et cetera*.), the discrete ℓ^2-inner product is defined by

$$\langle u^a, u^b \rangle_A = h^2 \sum_{j=1}^{N} \sum_{i=1}^{N} u^a_{i,j+1/2} u^b_{i,j+1/2}; \tag{2.9}$$

for any pair of variables v^a, v^b which are evaluated at the mesh points $(i + 1/2, j, j + 1/2)$, (such as v, $D_y\phi$, $D_y\mu$, $D_y p$, *et cetera.*), the discrete ℓ^2-inner product is defined by

$$\langle v^a, v^b \rangle_B = h^2 \sum_{j=1}^{N} \sum_{i=1}^{N} v^a_{i+1/2,\, j}\, v^b_{i+1/2,\, j}; \tag{2.10}$$

for any pair of variables μ^a, μ^b which are evaluated at the mesh points $(i + 1/2, j + 1/2)$, (such as μ, ϕ, p, *et cetera.*), the discrete ℓ^2-inner product is defined by

$$\langle \mu^a, \mu^b \rangle_C = h^2 \sum_{j=1}^{N} \sum_{i=1}^{N} \mu^a_{i+1/2,\, j+1/2}\, \mu^b_{i+1/2,\, j+1/2}. \tag{2.11}$$

In addition, for two velocity vector $\boldsymbol{u} = (u^x, u^y)^T$ and $\boldsymbol{v} = (v^x, v^y)^T$, we denote their vector inner product as

$$\langle \boldsymbol{u}, \boldsymbol{v} \rangle_1 = \langle u^x, v^x \rangle_A + \langle u^y, v^y \rangle_B. \tag{2.12}$$

Their ℓ^2 norms, namely, $\|\cdot\|_2$ norm, can be defined accordingly. Clearly all the discrete ℓ^2 inner products defined above are second order accurate. In addition to the standard L^2_h norm, we also introduce the ℓ^p, $1 \le p < \infty$, and ℓ^∞ norms for a grid function f evaluated at mesh points $(i + 1/2, j + 1/2)$:

$$\|f\|_\infty := \max_{i,j} |f_{i+1/2,\, j+1/2}|, \qquad \|f\|_p := \left(h^2 \sum_{i,j=1}^{N} |f_{i+1/2,\, j+1/2}|^p \right)^{\frac{1}{p}}, \quad 1 \le p < \infty. \tag{2.13}$$

The following summation by parts formulas will be useful in the later analysis.

Lemma 2.1 *For discrete grid functions* $\boldsymbol{u}$ *(evaluated at* $(x_i, y_{j+1/2})$*),* $\boldsymbol{v}$ *(evaluated at* $(x_{i+1/2}, y_j)$*),* μ*,* p*,* ϕ *(evaluated at* $(x_{i+1/2}, y_{j+1/2})$*) satisfying the discrete periodic boundary condition, the following identities are valid:*

$$\langle \boldsymbol{v}, \boldsymbol{u} \cdot \nabla_h \boldsymbol{v} \rangle_1 + \langle \boldsymbol{v}, \nabla_h \cdot (\boldsymbol{v}\boldsymbol{u}^T) \rangle_1 = 0, \tag{2.14}$$

$$\langle \boldsymbol{u}, \nabla_h p \rangle_1 = 0, \quad \text{if } \nabla_h \cdot \boldsymbol{u} = 0, \tag{2.15}$$

$$-\langle \boldsymbol{v}, \Delta_h \boldsymbol{v} \rangle_1 = \|\nabla_h \boldsymbol{v}\|_2^2 := \|\nabla_h v^x\|_1^2 + \|\nabla_h v^y\|_2^2, \tag{2.16}$$

$$-\langle \phi, \Delta_h \phi \rangle_C = \|\nabla_h \phi\|_2^2, \tag{2.17}$$

$$-\langle \mu, \nabla_h \cdot (\mathcal{A}_h \phi \boldsymbol{u}) \rangle_C = \langle \boldsymbol{u}, \mathcal{A}_h \phi \nabla_h \mu \rangle_1. \tag{2.18}$$

For any discrete grid function ϕ, the discrete version of the energy is defined as

$$E_h(\phi) := \langle (1+\phi)\ln(1+\phi) + (1-\phi)\ln(1-\phi), \mathbf{1} \rangle_C - \frac{\theta_0}{2}\|\phi\|_2^2 + \frac{\varepsilon^2}{2}\|\nabla_h \phi\|_2^2. \tag{2.19}$$

2.2 The Fully Discrete Numerical Scheme

The following finite difference scheme is proposed: given ϕ^n, $p^n \in \mathcal{C}_{\text{per}}$, $\mathbf{u}^n$ evaluated at the MAC staggered grid points, we find ϕ^{n+1}, $p^{n+1} \in \mathcal{C}_{\text{per}}$,$\mathbf{u}^{n+1}$ evaluated at the MAC

staggered grid points, such that

$$\frac{\bar{\mathbf{u}}^{n+1}-\mathbf{u}^n}{\Delta t}+\frac{1}{2}(\mathbf{u}^n\cdot\nabla_h\bar{\mathbf{u}}^{n+1}+\nabla_h\cdot(\bar{\mathbf{u}}^{n+1}(\mathbf{u}^n)^T)+\nabla_h p^n-\nu\Delta_h\bar{\mathbf{u}}^{n+1}$$
$$=-\gamma(\mathcal{A}_h\phi^n\nabla_h\mu^{n+1}), \tag{2.20}$$

$$\frac{\phi^{n+1}-\phi^n}{\Delta t}+\nabla_h\cdot(\mathcal{A}_h\phi^n\bar{\mathbf{u}}^{n+1})=\Delta_h\mu^{n+1}, \tag{2.21}$$

$$\mu^{n+1}=\ln(1+\phi^{n+1})-\ln(1-\phi^{n+1})-\theta_0\phi^n-\varepsilon^2\Delta_h\phi^{n+1}, \tag{2.22}$$

$$\frac{\mathbf{u}^{n+1}-\bar{\mathbf{u}}^{n+1}}{\Delta t}+\nabla_h(p^{n+1}-p^n)=0,\quad \nabla_h\cdot\mathbf{u}^{n+1}=0. \tag{2.23}$$

3 The Unique Solvability and Positivity Preserving Analysis

In the numerical solution to (2.20)–(2.23), it is observed that the phase variable is mass conservative, i.e.,

$$\overline{\phi^n}=\overline{\phi^0}:=\beta_0,\quad \text{with}\quad -1<\beta_0<1,\quad \forall\, n\geq 1, \tag{3.1}$$

in which the average operator is given by $\overline{f}=\frac{1}{|\Omega|}\langle f,\mathbf{1}\rangle_\Omega$. The following preliminary estimate, which was proved in a recent paper [7], is recalled.

Lemma 3.1 [7]. *Suppose that $\varphi^\star$, $\hat{\varphi}\in\mathcal{C}_{\text{per}}$, with $\hat{\varphi}-\varphi^\star\in\mathring{\mathcal{C}}_{\text{per}}$. Assume that $0<\hat{\varphi}_{i,j,k},\varphi^\star_{i,j,k}\leq M_h$, for all $1\leq i,j,k\leq N$, where $M_h>0$ may depend on h. The following estimate is valid:*

$$\|(-\Delta_h)^{-1}(\hat{\varphi}-\varphi^\star)\|_\infty\leq\tilde{C}_1 M_h, \tag{3.2}$$

where $\tilde{C}_1>0$ only depends on Ω.

To proceed with the unique solvability analysis, we implicitly define a linear operator $\mathcal{L}_h$ as follows. Assume that the fields $\mathbf{u}^n$, ϕ^n, and p^n are fixed. For a given field μ, $\mathbf{v}=\mathcal{L}_h\mu$ is the unique solution of the following discrete convection-diffusion equation:

$$\frac{\mathbf{v}-\mathbf{u}^n}{\Delta t}+\frac{1}{2}(\mathbf{u}^n\cdot\nabla_h\mathbf{v}+\nabla_h\cdot(\mathbf{v}(\mathbf{u}^n)^T))+\nabla_h p^n-\nu\Delta_h\mathbf{v}=-\gamma\mathcal{A}_h\phi^n\nabla_h\mu. \tag{3.3}$$

In fact, the linear operator $\mathcal{L}_h$ defined via (3.3) is an affine transform since it does not satisfy the homogeneous property and thus not preserve the linear combination, as demonstrated later. Given the time level t^n fields $(\mathbf{u}^n,\phi^n,p^n)$, we can represent $\bar{\mathbf{u}}^{n+1}=\mathcal{L}_h(\mu^{n+1})$. In turn, $\mathbf{u}^{n+1}$ becomes the discrete Helmholtz projection of $\bar{\mathbf{u}}^{n+1}$ into divergence-free space, which we express as $\mathbf{u}^{n+1}=\mathcal{P}_h\bar{\mathbf{u}}^{n+1}$. Subsequently, a substitution of $\bar{\mathbf{u}}^{n+1}=\mathcal{L}_h(\mu^{n+1})$ into (2.21) leads to the following system of equations for ϕ^{n+1} and μ^{n+1}:

$$\frac{\phi^{n+1}-\phi^n}{\Delta t}=-\nabla_h\cdot(\mathcal{A}_h\phi^n\mathcal{L}_h(\mu^{n+1}))+\Delta_h\mu^{n+1}, \tag{3.4}$$

$$\mu^{n+1}=\ln(1+\phi^{n+1})-\ln(1-\phi^{n+1})-\theta_0\phi^n-\varepsilon^2\Delta_h\phi^{n+1}. \tag{3.5}$$

Of course, (3.4) could be rewritten as

$$\frac{\phi^{n+1}-\phi^n}{\Delta t}=-\mathcal{G}_h(\mu^{n+1}), \tag{3.6}$$

$$\mathcal{G}_h(\mu) := \nabla_h \cdot (\mathcal{A}_h \phi^n \mathcal{L}_h \mu) - \Delta_h \mu. \tag{3.7}$$

Notice that $\mathcal{G}_h : (\mathbb{R}^{N^2})^2 \to (\mathbb{R}^{N^2})^2$ is a linear operator (with the discrete boundary condition imposed). Furthermore, this linear operator is invertible, as demonstrated by the following lemma.

Lemma 3.2 *The linear operator $\mathcal{G}_h$ satisfies the monotonicity condition:*

$$\langle \mathcal{G}_h(\mu^{(1)}) - \mathcal{G}_h(\mu^{(2)}), \mu^{(1)} - \mu^{(2)} \rangle_C \geq \|\nabla_h(\mu^{(1)} - \mu^{(2)})\|_2^2 \geq 0, \tag{3.8}$$

for any $\mu^{(1)}$, $\mu^{(2)}$. In addition, equality is realized if and only if $\mu^{(1)} = \mu^{(2)}$, if we require $\overline{\mu^{(1)}} = \overline{\mu^{(2)}} = 0$. Therefore, the operator $\mathcal{G}_h$ is invertible.

Proof A difference function is introduced as $\tilde{\mu} := \mu^{(1)} - \mu^{(2)}$. Since $\mathcal{G}_h$ is a linear operator, the following expansion is made:

$$\mathcal{G}_h(\mu^{(1)}) - \mathcal{G}_h(\mu^{(2)}) = \mathcal{G}_h(\tilde{\mu}) = \nabla_h \cdot (\mathcal{A}_h \phi^n \mathcal{L}_h \tilde{\mu}) - \Delta_h \tilde{\mu}. \tag{3.9}$$

Taking a discrete inner product with (3.9) by $\tilde{\mu}$ yields

$$\langle \mathcal{G}_h(\tilde{\mu}), \tilde{\mu} \rangle_C = -\langle \mathcal{A}_h \phi^n \nabla_h \tilde{\mu}, \mathcal{L}_h \tilde{\mu} \rangle_1 + \|\nabla_h \tilde{\mu}\|_2^2. \tag{3.10}$$

Meanwhile, we define $\mathbf{v}^{(i)} := \mathcal{L}_h(\mu^{(i)})$, $i = 1, 2$, and $\tilde{\mathbf{v}} := \mathbf{v}^{(1)} - \mathbf{v}^{(2)} = \mathcal{L}_h \tilde{\mu}$, using the linearity of $\mathcal{L}_h$. In addition, the definition of $\mathcal{L}_h$ in (3.3) implies that

$$\frac{\tilde{\mathbf{v}}}{\Delta t} + \frac{1}{2}(\mathbf{u}^n \cdot \nabla_h \tilde{\mathbf{v}} + \nabla_h \cdot (\tilde{\mathbf{v}}(\mathbf{u}^n)^T)) - \nu \Delta_h \tilde{\mathbf{v}} + \gamma \mathcal{A}_h \phi^n \nabla_h \tilde{\mu} = 0. \tag{3.11}$$

The non-homogeneous source terms, namely $\frac{\mathbf{u}^n}{\Delta t}$ and $\nabla_h p^n$, vanish in this difference equation, since $\tilde{\mathbf{v}}$ is the difference of the two solutions $\mathbf{v}^{(1)}$ and $\mathbf{v}^{(2)}$. Subsequently, taking a discrete inner product with (3.11) by $\tilde{\mathbf{v}} = \mathcal{L}_h \tilde{\mu}$ leads to

$$\frac{1}{\Delta t}\|\tilde{\mathbf{v}}\|_2^2 + \nu \|\nabla_h \tilde{\mathbf{v}}\|_2^2 + \gamma \langle (\mathcal{A}_h \phi^n \nabla_h \tilde{\mu}, \mathcal{L}_h \tilde{\mu} \rangle_1 = 0, \tag{3.12}$$

in which we have made use of the following identities:

$$\langle \mathbf{u}^n \cdot \nabla_h \tilde{\mathbf{v}} + \nabla_h \cdot (\tilde{\mathbf{v}}(\mathbf{u}^n)^T), \tilde{\mathbf{v}} \rangle_1 = 0, \tag{3.13}$$

$$-(\tilde{\mathbf{v}}, \Delta_h \tilde{\mathbf{v}}) = \|\nabla_h \tilde{\mathbf{v}}\|_2^2. \tag{3.14}$$

Consequently, a combination of (3.12) and (3.10) leads to

$$\langle \mathcal{G}_h(\tilde{\mu}), \tilde{\mu} \rangle_C = \frac{1}{\gamma}\left(\frac{1}{\Delta t}\|\tilde{\mathbf{v}}\|_2^2 + \nu \|\nabla_h \tilde{\mathbf{v}}\|_2^2\right) + \|\nabla_h \tilde{\mu}\|_2^2, \tag{3.15}$$

which is equivalent to

$$\begin{aligned} \langle \mathcal{G}_h(\mu^{(1)}) - \mathcal{G}_h(\mu^{(2)}), \mu^{(1)} - \mu^{(2)} \rangle_C &= \langle \mathcal{G}_h(\tilde{\mu}), \tilde{\mu} \rangle_C \geq \|\nabla_h \tilde{\mu}\|_2^2 \\ &= \|\nabla_h(\mu^{(1)} - \mu^{(2)})\|_2^2 \geq 0, \end{aligned} \tag{3.16}$$

so that (3.8) has been proved. In addition, it is clear that equality is valid if and only if $\tilde{\mu} \equiv 0$, i.e., $\mu^{(1)} = \mu^{(2)}$, under the requirement that $\overline{\mu^{(1)}} = \overline{\mu^{(2)}} = 0$. The proof is complete. □

Since the linear operator $\mathcal{G}_h$ maps $(\mathbb{R}^{N^2})^2$ into $(\mathbb{R}^{N^2})^2$, we see that the inverse operator $\mathcal{G}_h^{-1}$ also maps $(\mathbb{R}^{N^2})^2$ into $(\mathbb{R}^{N^2})^2$. As a direct consequence of Lemma 3.2, the following result is available.

Proposition 3.1 *The linear operator $\mathcal{G}_h^{-1}$ also satisfies the monotonicity condition:*

$$\begin{aligned}\langle \mathcal{G}_h^{-1}(\phi^{(1)}) - \mathcal{G}_h^{-1}(\phi^{(2)}), \phi^{(1)} - \phi^{(2)} \rangle_C &\geq \|\nabla_h(\mathcal{G}_h^{-1}(\phi^{(1)} - \phi^{(2)}))\|_2^2 \\ &\geq C_1^2 \|\mathcal{G}_h^{-1}(\phi^{(1)} - \phi^{(2)}))\|_2^2, \end{aligned} \tag{3.17}$$

for any $\phi^{(1)}$, $\phi^{(2)}$, with $\overline{\phi^{(1)}} = \overline{\phi^{(2)}} = 0$. The constant C_1 is associated with the discrete elliptic regularity

$$\|\nabla_h f\|_2 \geq C_1 \|f\|_2, \quad \text{for any } f \text{ with } \overline{f} = 0, \text{ with } C_1 \text{ only dependent on } \Omega. \tag{3.18}$$

In addition, the equality is valid if and only if $\phi^{(1)} = \phi^{(2)}$.

Proof We denote $\mu^{(i)} = \mathcal{G}_h^{-1}(\phi^{(i)})$, $i = 1, 2$, which is equivalent to $\phi^{(i)} = \mathcal{G}_h \mu^{(i)}$, $i = 1, 2$. An application of (3.8) reveals that

$$\begin{aligned}\langle \mathcal{G}_h^{-1}(\phi^{(1)}) - \mathcal{G}_h^{-1}(\phi^{(2)}), \phi^{(1)} - \phi^{(2)} \rangle_C &= \langle \mathcal{G}_h(\mu^{(1)}) - \mathcal{G}_h(\mu^{(2)}), \mu^{(1)} - \mu^{(2)} \rangle_C \\ &\geq \|\nabla_h(\mu^{(1)} - \mu^{(2)})\|_2^2 \geq C_1^2 \|\mu^{(1)} - \mu^{(2)}\|_2^2 \\ &= C_1^2 \|\mathcal{G}_h^{-1}(\phi^{(1)} - \phi^{(2)})\|_2^2 \geq 0. \end{aligned} \tag{3.19}$$

Clearly, the equality is valid if and only if $\phi^{(1)} = \phi^{(2)}$. This finishes the proof for Proposition 3.1. □

By the construction (3.3) and the definition (3.7) for the operator $\mathcal{G}_h$, it is observed that the following homogenization formula is available:

$$\mathcal{G}_h(\mu) = \mathcal{G}_h^{(0)} + \mathcal{G}_h^*(\mu), \quad \mathcal{G}_h^{(0)} = \nabla_h \cdot (\mathcal{A}_h \phi^n (\mathbf{u}^n - \Delta t \nabla_h p^n)), \quad \text{for any } \overline{\mu} = 0, \tag{3.20}$$

in which $\mathcal{G}_h^*$ corresponds to a homogeneous linear operator. In fact, this operator satisfies the linearity property as in the standard definition, in comparison with the operator $\mathcal{L}_h$ given by (3.3). In addition, the following bound is assumed for the non-homogeneous source term, which only depends on the numerical solution at the previous time step:

$$\|\mathcal{G}_h^{(0)}\|_2 \leq A^*. \tag{3.21}$$

Proposition 3.2 *For any φ with $\overline{\varphi} = 0$, the following $\|\cdot\|_2$ and $\|\cdot\|_\infty$ bounds are valid:*

$$\|\mathcal{G}_h^{-1}(\varphi)\|_2 \leq C_1^{-2}(\|\varphi\|_2 + A^*), \tag{3.22}$$

$$\|\mathcal{G}_h^{-1}(\varphi)\|_\infty \leq C C_1^{-2} h^{-\frac{3}{2}}(\|\varphi\|_2 + A^*). \tag{3.23}$$

Proof For any φ with $\overline{\varphi} = 0$, we denote $\mu = \mathcal{G}_h^{-1}(\varphi)$. By the homogenization decomposition (3.20), it is clear that $\mathcal{G}_h^*(\mu) = \psi := \varphi - \mathcal{G}_h^{(0)}$. Meanwhile, the monotonicity inequality (3.8) implies that

$$\begin{aligned}\langle \mathcal{G}_h^*(\mu), \mu \rangle_C &\geq \|\nabla_h \mu\|_2^2 \geq C_1^2 \|\mu\|_2^2, \quad \text{so that} \\ \|\mu\|_2^2 &\leq C_1^{-2} \langle \mathcal{G}_h^*(\mu), \mu \rangle_C \leq C_1^{-2} \|\mathcal{G}_h^*(\mu)\|_2 \cdot \|\mu\|_2, \\ \|\mu\|_2 &\leq C_1^{-2} \|\mathcal{G}_h^*(\mu)\|_2, \end{aligned} \tag{3.24}$$

in which the Cauchy inequality has been applied. Then we arrive at

$$\begin{aligned}\|\mathcal{G}_h^{-1}(\varphi)\|_2 = \|\mu\|_2 &\leq C_1^{-2} \|\mathcal{G}_h^*(\mu)\|_2 = C_1^{-2} \|\varphi - \mathcal{G}_h^{(0)}\|_2 \\ &\leq C_1^{-2}(\|\varphi\|_2 + \|\mathcal{G}_h^{(0)}\|_2), \end{aligned} \tag{3.25}$$

which is exactly (3.22). Furthermore, the $\|\cdot\|_\infty$ estimate (3.23) comes from a direct application of 3-D inverse inequality. This finishes the proof of Proposition 3.2. □

By (3.4), (3.5) and (3.6), (3.7), it is clear that the numerical solution (2.20)–(2.22) could be equivalently represented as the following nonlinear system, in terms of ϕ^{n+1}:

$$\mu^{n+1} + \frac{1}{\Delta t}\mathcal{G}_h^{-1}(\phi^{n+1} - \phi^n) = \ln(1+\phi^{n+1}) - \ln(1-\phi^{n+1}) - \theta_0\phi^n - \varepsilon^2\Delta_h\phi^{n+1} + \frac{1}{\Delta t}\mathcal{G}_h^{-1}(\phi^{n+1} - \phi^n) = 0. \tag{3.26}$$

Meanwhile, it is observed that $\mathcal{G}_h^{-1}$ is not a symmetric operator, although it is monotone. Because of this non-symmetric feature, we are not able to represent the numerical solution of (3.26) as a minimization of certain discrete energy functional in terms of of ϕ^{n+1}.

To overcome this subtle difficulty, we observe the fact that, with a given field g, the unique solvability and positivity preserving analysis of the following nonlinear system, for any $A \geq 0$, could be established in the same manner as in a recent work [7]:

$$\ln(1+\phi) - \ln(1-\phi) - \theta_0\phi^n - \varepsilon^2\Delta_h\phi + A\phi = g. \tag{3.27}$$

In fact, the implicit part of ϕ corresponds to a strictly convex energy functional:

$$J_h^n(\phi) = \langle (1+\phi)\ln(1+\phi) + (1-\phi)\ln(1-\phi), \mathbf{1}\rangle_C + \frac{\varepsilon^2}{2}\|\nabla_h\phi\|_2^2 - \langle g + \theta_0\phi^n, \phi\rangle_C. \tag{3.28}$$

The positivity preserving and unique solvability analysis of the numerical solution (3.27), for a given g, is stated in the following proposition. The proof is skipped for the sake of brevity, and the technical details are left to interested readers.

Proposition 3.3 *Given $\phi^n \in \mathcal{C}_{\rm per}$, with $-1 < \phi^n_{i,j,k} < 1$, $1 \leq i, j, k \leq N$, and $\overline{\phi^n} = \beta_0$, there exists a unique solution $\phi \in \mathcal{C}_{\rm per}$ to (3.27), with $0 < \phi_{i,j,k}$, $1 \leq i, j, k \leq N$ and $\overline{\phi} = \beta_0$. In addition, the following lower bound for the numerical solution is available, at a point-wise level:*

$$1+\phi,\ 1-\phi \geq \delta^*, \quad \text{so that} \quad \ln\delta^* - \ln\frac{\beta_0}{2-\beta_0} + \frac{12\varepsilon^2}{h^2} + \|g + \theta_0\phi^n\|_\infty = 0. \tag{3.29}$$

Remark 3.1 The technique of positivity preserving analysis has been successfully applied to various gradient flow models, such as the Cahn-Hilliard equation with Flory-Huggins energy potential [5, 7, 12–14, 48], the liquid film droplet model [49], the Poisson-Nernst-Planck system [37, 38, 42], the reaction-diffusion system with detailed balance [36], etc. In these works, the convex nature of the energy functional associated with singular term has played an essential role. This feature prevents the numerical solution approach the singular limit value of 0, which turns out to be the key point in the analysis.

Of course, in the rewritten form of the numerical solution (3.26), $g = -\frac{1}{\Delta t}\mathcal{G}_h^{-1}(\phi - \phi^n)$ is coupled with the left hand side. The unique solvability and positivity preserving analysis for the proposed numerical scheme is stated in the following theorem.

Theorem 3.1 *Given $\phi^n \in \mathcal{C}_{\rm per}$, with $-1 < \phi^n_{i,j,k} < 1$, $1 \leq i, j, k \leq N$, $\overline{\phi^n} = \beta_0$, there exists a unique solution $\phi^{n+1} \in \mathcal{C}_{\rm per}$ to (2.20)–(2.23), or equivalently (3.26), with $-1 < \phi^{n+1}_{i,j,k} < 1$, $1 \leq i, j, k \leq N$, and $\overline{\phi^{n+1}} = \beta_0$.*

Proof The existence of the numerical solution for (3.26) is proved by an iteration approach. Given the m^{th} iterate $\rho^{(m)} \in \mathcal{C}_{\text{per}}$, with $0 < \rho_{i,j,k}^{(m)}$, $1 \le i, j, k \le N$, and $\overline{\rho^{(m)}} = \beta_0$, the following nonlinear iteration is constructed:

$$\begin{aligned} B_h^*(\phi^{(m+1)}) &:= \ln(1+\phi^{(m+1)}) - \ln(1-\phi^{(m+1)}) - \varepsilon^2 \Delta_h \phi^{(m+1)} + A\phi^{(m+1)} - \theta_0 \phi^n \\ &= -\frac{1}{\Delta t} \mathcal{G}_h^{-1}(\phi^{(m)} - \phi^n) + A\phi^{(m)}. \end{aligned} \tag{3.30}$$

In fact, Proposition 3.3 has implied a point-wise positive solution $\phi^{(m+1)}$ for any given $\mathcal{G}_h^{-1}(\phi^{(m)} - \phi^n)$.

In the next step, we aim to establish the contraction mapping property of the nonlinear iteration (3.30), for a sufficiently large A. The following difference function is introduced, between two consecutive iteration stages:

$$e^{(m)} := \phi^{(m)} - \phi^{(m-1)}, \quad \text{for } m \ge 1. \tag{3.31}$$

It is clear that $\overline{e^{(m)}} = 0$, due to the fact that $\overline{\phi^{(m)}} = \overline{\phi^{(m-1)}} = \beta_0$, for any $m \ge 1$. Subsequently, an application of discrete elliptic regularity (3.18) gives

$$\|\nabla_h e^{(m)}\|_2 \ge C_1 \|e^{(m)}\|_2, \quad \forall m \ge 1. \tag{3.32}$$

Taking a difference of (3.30) between the m^{th} and the $(m+1)^{\text{st}}$ iteration stages leads to

$$\begin{aligned} B_h^*(\phi^{(m+1)}) - B_h^*(\phi^{(m)}) &= \ln(1+\phi^{(m+1)}) - \ln(1+\phi^{(m)}) - \ln(1-\phi^{(m+1)}) \\ &\quad + \ln(1-\phi^{(m)}) + Ae^{(m+1)} - \varepsilon^2 \Delta_h e^{(m+1)} \\ &= -\frac{1}{\Delta t} \mathcal{G}_h^{-1}(\phi^{(m)} - \phi^{(m-1)}) + Ae^{(m)}. \end{aligned} \tag{3.33}$$

In turn, taking a discrete inner product with (3.33) by $e^{(m+1)}$ results in

$$\begin{aligned} &\langle \ln(1+\phi^{(m+1)}) - \ln(1+\phi^{(m)}), e^{(m+1)} \rangle_C + \langle -\ln(1-\phi^{(m+1)}) + \ln(1-\phi^{(m)}), e^{(m+1)} \rangle_C \\ &\quad + A\langle e^{(m+1)} - e^{(m)}, e^{(m+1)} \rangle + \varepsilon^2 \|\nabla_h e^{(m+1)}\|_2^2 \\ &= -\frac{1}{\Delta t} \left\langle \mathcal{G}_h^{-1}(\phi^{(m)} - \phi^{(m-1)}), e^{(m+1)} \right\rangle_C. \end{aligned} \tag{3.34}$$

The nonlinear inner products on the left hand side are always non-negative, due to the monotone property of the logarithmic function:

$$\begin{aligned} &\langle \ln(1+\phi^{(m+1)}) - \ln(1+\phi^{(m)}), e^{(m+1)} \rangle_C \\ &\quad = \langle \ln(1+\phi^{(m+1)}) - \ln(1+\phi^{(m)}), \phi^{(m+1)} - \phi^{(m)} \rangle_C \ge 0. \end{aligned} \tag{3.35}$$

$$\langle -\ln(1-\phi^{(m+1)}) + \ln(1+\phi^{(m)}), e^{(m+1)} \rangle_C \ge 0, \quad \text{(similar analysis)}. \tag{3.36}$$

For the iteration relaxation term, the following identity is available:

$$\langle e^{(m+1)} - e^{(m)}, e^{(m+1)} \rangle_C = \frac{1}{2}(\|e^{(m+1)}\|_2^2 - \|e^{(m)}\|_2^2 + \|e^{(m+1)} - e^{(m)}\|_2^2). \tag{3.37}$$

Going back (3.34), we get

$$\begin{aligned} &\frac{A}{2}\|e^{(m+1)}\|_2^2 + \frac{A}{2}\|e^{(m+1)} - e^{(m)}\|_2^2 + \varepsilon^2 \|\nabla_h e^{(m+1)}\|_2^2 \\ &\quad \le \frac{A}{2}\|e^{(m)}\|_2^2 - \frac{1}{\Delta t} \left\langle \mathcal{G}_h^{-1}(\phi^{(m)} - \phi^{(m-1)}), e^{(m+1)} \right\rangle_C. \end{aligned} \tag{3.38}$$

For the right hand side inner product, we begin with the following decomposition:

$$-\left\langle \mathcal{G}_h^{-1}(\phi^{(m)}-\phi^{(m-1)}), e^{(m+1)}\right\rangle_C = -\left\langle \mathcal{G}_h^{-1}(\phi^{(m)}-\phi^{(m-1)}), e^{(m)}\right\rangle_C - \left\langle \mathcal{G}_h^{-1}(\phi^{(m)}-\phi^{(m-1)}), e^{(m+1)}-e^{(m)}\right\rangle_C. \quad (3.39)$$

The first part is always non-positive, with an application of the monotonicity analysis (3.17) (in Proposition 3.1):

$$-\left\langle \mathcal{G}_h^{-1}(\phi^{(m)}-\phi^{(m-1)}), e^{(m)}\right\rangle_C = -\left\langle \mathcal{G}_h^{-1}(\phi^{(m)}-\phi^{(m-1)}), \phi^{(m)}-\phi^{(m-1)}\right\rangle_C \le 0. \quad (3.40)$$

Moreover, the monotonicity analysis (3.17) reveals that

$$\|\mathcal{G}_h^{-1}(\phi^{(m)}-\phi^{(m-1)})\|_2 \le C_1^{-2}\|\phi^{(m)}-\phi^{(m-1)}\|_2 = C_1^{-2}\|e^{(m)}\|_2, \quad (3.41)$$

so that the following estimate is valid for the second part:

$$\begin{aligned} -\left\langle \mathcal{G}_h^{-1}(\phi^{(m)}-\phi^{(m-1)}), e^{(m+1)}-e^{(m)}\right\rangle_C &\le \|\mathcal{G}_h^{-1}(\phi^{(m)}-\phi^{(m-1)})\|_2 \cdot \|e^{(m+1)}-e^{(m)}\|_2 \\ &\le C_1^{-2}\|e^{(m)}\|_2 \cdot \|e^{(m+1)}-e^{(m)}\|_2. \end{aligned} \quad (3.42)$$

In turn, a substitution of (3.40) and (3.42) into (3.39) yields

$$\begin{aligned} -\frac{1}{\Delta t}\left\langle \mathcal{G}_h^{-1}(\phi^{(m)}-\phi^{(m-1)}), e^{(m+1)}\right\rangle_C &\le C_1^{-2}\Delta t^{-1}\|e^{(m)}\|_2 \cdot \|e^{(m+1)}-e^{(m)}\|_2 \\ &\le \frac{\varepsilon^2}{2}C_1^2\|e^{(m)}\|_2^2 + \frac{1}{2}C_1^{-6}\varepsilon^{-2}\Delta t^{-2}\|e^{(m+1)}-e^{(m)}\|_2^2. \end{aligned} \quad (3.43)$$

A combination of (3.38) and (3.43) yields

$$\begin{aligned} &(\frac{A}{2}+C_1^2\varepsilon^2)\|e^{(m+1)}\|_2^2 + \frac{A}{2}\|e^{(m+1)}-e^{(m)}\|_2^2 \\ &\le (\frac{A}{2}+\frac{\varepsilon^2}{2}C_1^2)\|e^{(m)}\|_2^2 + \frac{1}{2}C_1^{-6}\varepsilon^{-2}\Delta t^{-2}\|e^{(m+1)}-e^{(m)}\|_2^2. \end{aligned} \quad (3.44)$$

As a result, by taking $A = C_1^{-6}\varepsilon^{-2}\Delta t^{-2}$, a fixed constant which may depend on Δt, Ω and ε, we arrive at the following iteration estimate:

$$(\frac{A}{2}+C_1^2\varepsilon^2)\|e^{(m+1)}\|_2^2 \le (\frac{A}{2}+\frac{1}{2}C_1^2\varepsilon^2)\|e^{(m)}\|_2^2. \quad (3.45)$$

In other words, the nonlinear iteration (3.30) is assured to be a contraction mapping, by taking $A = C_1^{-6}\varepsilon^{-2}\Delta t^{-2}$. As a consequence, such a nonlinear process must have a convergence solution in the fixed point iteration, and the limit convergence solution is exactly the solution to (3.26), or equivalently, the numerical system (2.20)–(2.22). The existence of the proposed numerical scheme is proved.

In addition, since the operator B_h corresponds to a strictly convex energy, and the linear operator $\mathcal{G}_h^{-1}(\phi)$ is monotone (in terms of ϕ), the uniqueness analysis for the numerical solution of (3.26) follows a standard monotonicity analysis.

After the unique intermediate velocity vector $\bar{\mathbf{u}}^{n+1}$, the numerical vector $\mathbf{u}^{n+1}$ turns out to be the discrete Helmholtz projection of $\bar{\mathbf{u}}^{n+1}$ into the divergence-free vector space, which is equivalent to a discrete Poisson solver. The proof of Theorem 3.1 is complete. □

Meanwhile, the Browder–Minty lemma is recalled as follows.

Lemma 3.3 (Browder–Minty [1, 41]) *Let X be a real, reflexive Banach space and suppose X' is its dual. Let $T : X \to X'$ be (i) bounded; (ii) continuous; (iii) coercive, that is,*

$$\frac{\langle T(u), u\rangle}{\|u\|_X} \to +\infty \quad as \quad \|u\|_X \to +\infty; \tag{3.46}$$

and (iv) monotone. Then for any $g \in X'$ there exists a solution $u \in X$ of the equation $T(u) = g$. Furthermore, if the operator T is strictly monotone, then the solution u is unique.

Remark 3.2 In fact, the numerical solution (3.26) could be equivalently rewritten as follows

$$\begin{aligned} F_h(\phi^{n+1}) :=\ & B_h(\phi^{n+1}) + \frac{1}{\Delta t}\mathcal{G}_h^{-1}(\phi^{n+1} - \phi^n) \\ =\ & \ln(1+\phi^{n+1}) - \ln(1-\phi^{n+1}) \\ & -\theta_0\phi^n - \varepsilon^2\Delta_h\phi^{n+1} + \frac{1}{\Delta t}\mathcal{G}_h^{-1}(\phi^{n+1} - \phi^n) = 0. \end{aligned} \tag{3.47}$$

The monotone property of $F_h(\phi)$ could be derived in a straightforward manner. However, the Browder–Minty lemma is not directly applicable for this numerical system, due to the fact that $\ln(1 \pm \phi)$ becomes singular as $\phi \to -1+$ or $\phi \to 1-$, so that the coercivity condition of the operator F_h could not be verified. Instead, the nonlinear iteration (3.30) is constructed, and a contraction mapping property is theoretically justified, so that the convergence limit of the fixed-point iteration turns out to be the solution of the numerical system (3.26).

Remark 3.3 At each fixed iteration stage, given by (3.30), it is clear that $g = -\frac{1}{\Delta t}\mathcal{G}_h^{-1}(\phi^{(m)} - \phi^n) + A\phi^{(m)}$. In addition, the $\|\cdot\|_\infty$ estimate (3.23) (in Proposition 3.2) implies that

$$\begin{aligned} \|\mathcal{G}_h^{-1}(\phi^{(m)} - \phi^n)\|_\infty &\le CC_1^{-2}h^{-\frac{3}{2}}(\|\phi^{(m)} - \phi^n\|_2 + A^*) \\ &\le CC_1^{-2}h^{-\frac{3}{2}}(A^* + 2|\Omega|^{\frac{1}{2}}), \end{aligned} \tag{3.48}$$

in which the last step comes from the fact that $-1 < \phi^{(m)}, \phi^n < 1$ at a point-wise level. This in turn gives

$$\begin{aligned} \|g\|_\infty &\le \frac{1}{\Delta t}\|\mathcal{G}_h^{-1}(\phi^{(m)} - \phi^n)\|_\infty + A\|\phi^{(m)}\|_\infty \\ &\le CC_1^{-2}(A^* + 2|\Omega|^{\frac{1}{2}})\Delta t^{-1}h^{-\frac{3}{2}} + A, \end{aligned} \tag{3.49}$$

$$\begin{aligned} \|g + \theta_0\phi^n\|_\infty &\le \|g\|_\infty + \theta_0\|\phi^n\|_\infty \le B^* \\ &:= CC_1^{-2}(A^* + 2|\Omega|^{\frac{1}{2}})\Delta t^{-1}h^{-\frac{3}{2}} + A + \theta_0. \end{aligned} \tag{3.50}$$

As a result, by the point-wise lower bound estimate (3.29) (in Proposition 3.3), we conclude that

$$1 + \phi^{(m+1)},\ 1 - \phi^{(m+1)} \ge \delta^*, \quad \text{with} \quad \ln\delta^* - \ln\frac{\beta_0}{2-\beta_0} + \frac{12\varepsilon^2}{h^2} + B^* = 0. \tag{3.51}$$

This lower bound δ^* only depends on $\Delta t, h, \Omega, \mathbf{u}^n, \phi^n, p^n$ and β_0, while it is viewed as a fixed distance between $1 + \phi^{(m+1)}$ and $1 - \phi^{(m+1)}$ and the singular limit value 0, with all these given parameters and the numerical solution at the previous time step, at any iteration stage. Because of this lower bound, the point-wise convergence of the iteration solution $\phi^{(m+1)}$, ensured by the contraction mapping property (3.45), would not create a singular limit, so that the point-wise positivity property is valid for the numerical solution of (3.30).

Remark 3.4 We also point out that the iteration method utilized in the existence proof can be formulated into a somewhat more general form as

$$N(u^{n+1}) + L_s u^{n+1} + R u^{n+1} = f - L_a u^n + R u^n,$$

where N is a nonlinear monotone operator that satisfies the conditions in the Minty-Browder theorem, L_s is a symmetric coercive linear operator, L_a is a (non-symmetric) and continuous linear operator, and R is an appropriate regularization parameter. We leave the details to the interested reader.

Remark 3.5 Periodic boundary conditions have been assumed throughout the analysis for simplicity. A more careful analysis reveals that the positivity-preserving property remains true even if we impose Neumann boundary condition for the phase variable, together with a no-slip or free-slip boundary condition for the velocity. In another word, this analysis is independent of the boundary condition for either the phase variable or the velocity vector, and any boundary condition (even if it is non-homogeneous) coupled with the fluid solver operator $\mathcal{L}_h$ would lead to the same estimate of the desired result. This will significantly enhance the general availability of the positivity-preserving analysis presented in this paper.

4 Energy Stability Analysis

With the positivity-preserving and unique solvability properties for the numerical scheme (2.20)–(2.23) established, a total energy dissipation law could be derived. The following discrete phase field energy is introduced:

$$E_h(\phi) := \langle (1+\phi)\ln(1+\phi) + (1-\phi)\ln(1-\phi), \mathbf{1}\rangle_C - \frac{\theta_0}{2}\|\phi\|_2^2 + \frac{\varepsilon^2}{2}\|\nabla_h \phi\|_2^2. \quad (4.1)$$

Theorem 4.1 *For the numerical solution* (2.20)–(2.23)*, we have*

$$\begin{aligned} &\widetilde{E}_h(\phi^{n+1}, \mathbf{u}^{n+1}, p^{n+1}) + \frac{\nu \Delta t}{\gamma}\|\nabla_h \bar{\mathbf{u}}^{n+1}\|_2^2 + \Delta t \|\nabla_h \mu^{n+1}\|_2^2 \le \widetilde{E}_h(\phi^n, \mathbf{u}^n, p^n), \\ &\widetilde{E}_h(\phi^n, \mathbf{u}^n, p^n) := E_h(\phi^n) + \frac{1}{2\gamma}\|\mathbf{u}^n\|_2^2 + \frac{\Delta t^2}{2\gamma}\|\nabla_h p^n\|_2^2, \end{aligned} \quad (4.2)$$

so that $\widetilde{E}_h(\phi^m, \mathbf{u}^m, p^m) \le \widetilde{E}_h(\phi^0, \mathbf{u}^0, p^0) \le Q_0$*, for all* $m \in \mathbb{N}$*, where* $Q_0 > 0$ *is a constant independent of* h*.*

Proof Taking discrete inner products with (2.20) by $\bar{\mathbf{u}}^{n+1}$, (2.21) by μ^{n+1}, leads to

$$\begin{aligned} &\frac{1}{2\Delta t}(\|\bar{\mathbf{u}}^{n+1}\|_2^2 - \|\mathbf{u}^n\|_2^2 + \|\bar{\mathbf{u}}^{n+1} - \mathbf{u}^n\|_2^2) \\ &\quad + \nu\|\nabla_h \bar{\mathbf{u}}^{n+1}\|_2^2 + \langle \nabla_h p^n, \bar{\mathbf{u}}^{n+1}\rangle_1 \\ &\quad = -\gamma \langle \mathcal{A}_h \phi^n \nabla_h \mu^{n+1}, \bar{\mathbf{u}}^{n+1}\rangle_1, \end{aligned} \quad (4.3)$$

$$\begin{aligned} \langle \phi^{n+1} - \phi^n, \mu^{n+1}\rangle_C &= \langle \phi^{n+1} - \phi^n, \ln(1+\phi^{n+1}) \\ &\quad - \ln(1-\phi^{n+1}) - \theta_0 \phi^n - \varepsilon^2 \Delta_h \phi^{n+1}\rangle_C \\ &= \Delta t \langle \mathcal{A}_h \phi^n \nabla_h \mu^{n+1}, \bar{\mathbf{u}}^{n+1}\rangle_1 - \Delta t \|\nabla_h \mu^{n+1}\|_2^2. \end{aligned} \quad (4.4)$$

Meanwhile, the convexity of the discrete energy terms, $\langle (1+\phi)\ln(1+\phi), \mathbf{1}\rangle_C$, $\langle (1-\phi)\ln(1-\phi), \mathbf{1}\rangle_C$, $\|\phi\|_2^2$ and $\|\nabla_h \phi\|_2^2$ (in terms of ϕ), reveals that

$$\langle \phi^{n+1}-\phi^n, \ln(1+\phi^{n+1})\rangle_C \geq \big\langle (1+\phi^{n+1})\ln(1+\phi^{n+1}), \mathbf{1}\big\rangle - \big\langle (1+\phi^n)\ln(1+\phi^n), \mathbf{1}\big\rangle, \tag{4.5}$$

$$\langle \phi^{n+1}-\phi^n, -\ln(1-\phi^{n+1})\rangle_C \geq \big\langle (1-\phi^{n+1})\ln(1-\phi^{n+1}), \mathbf{1}\big\rangle - \big\langle (1-\phi^n)\ln(1-\phi^n), \mathbf{1}\big\rangle, \tag{4.6}$$

$$\langle \phi^{n+1}-\phi^n, -\phi^n\rangle_C \geq -\frac{1}{2}(\|\phi^{n+1}\|_2^2 - \|\phi^n\|_2^2), \tag{4.7}$$

$$\langle \phi^{n+1}-\phi^n, -\Delta_h \phi^{n+1}\rangle_C \geq \frac{1}{2}(\|\nabla_h \phi^{n+1}\|_2^2 - \|\nabla_h \phi^n\|_2^2). \tag{4.8}$$

Consequently, a substitution of (4.5)–(4.8) into (4.3) and (4.4) leads to

$$\begin{aligned} &E_h(\phi^{n+1}) - E_h(\phi^n) + \frac{1}{2\gamma}(\|\bar{\mathbf{u}}^{n+1}\|_2^2 - \|\mathbf{u}^n\|_2^2) \\ &+ \frac{\nu\Delta t}{\gamma}\|\nabla_h \bar{\mathbf{u}}^{n+1}\|_2^2 + \Delta t\|\nabla_h \mu^{n+1}\|_2^2 + \frac{\Delta t}{\gamma}\langle \nabla_h p^n, \bar{\mathbf{u}}^{n+1}\rangle_1 \leq 0. \end{aligned} \tag{4.9}$$

Regarding the term $\langle \nabla_h p^n, \overline{\boldsymbol{u}}^{n+1}\rangle_1$, the following identity is available:

$$\begin{aligned} \langle \nabla_h p^n, \bar{\mathbf{u}}^{n+1}\rangle_1 &= -\langle p^n, \nabla_h \cdot \bar{\mathbf{u}}^{n+1}\rangle_C = -\langle p^n, \Delta t \Delta_h (p^{n+1}-p^n)\rangle_C \\ &= \Delta t \langle \nabla_h p^n, \nabla_h (p^{n+1}-p^n)\rangle_1 \\ &= \frac{\Delta t}{2}(\|\nabla_h p^{n+1}\|_2^2 - \|\nabla_h p^n\|_2^2) - \frac{\Delta t}{2}\|\nabla_h (p^{n+1}-p^n)\|_2^2 \\ &= \frac{\Delta t}{2}(\|\nabla_h p^{n+1}\|_2^2 - \|\nabla_h p^n\|_2^2) - \frac{1}{2\Delta t}\|\boldsymbol{u}^{n+1} - \overline{\boldsymbol{u}}^{n+1}\|_2^2, \end{aligned} \tag{4.10}$$

where (2.23) has been applied in the derivation. A substitution of (4.10) into (4.9) yields

$$\begin{aligned} &E_h(\phi^{n+1}) - E_h(\phi^n) + \frac{1}{2\gamma}(\|\bar{\mathbf{u}}^{n+1}\|_2^2 - \|\mathbf{u}^n\|_2^2) + \frac{\nu\Delta t}{\gamma}\|\nabla_h \bar{\mathbf{u}}^{n+1}\|_2^2 + \Delta t\|\nabla_h \mu^{n+1}\|_2^2 \\ &+ \frac{\Delta t^2}{2\gamma}(\|\nabla_h p^{n+1}\|_2^2 - \|\nabla_h p^n\|_2^2) - \frac{1}{2\gamma}\|\mathbf{u}^{n+1} - \bar{\mathbf{u}}^{n+1}\|_2^2 \leq 0. \end{aligned} \tag{4.11}$$

On the other hand, taking a discrete inner product with (2.23) by $\mathbf{u}^{n+1}$ results in

$$\|\mathbf{u}^{n+1}\|_2^2 - \|\bar{\mathbf{u}}^{n+1}\|_2^2 + \|\mathbf{u}^{n+1} - \bar{\mathbf{u}}^{n+1}\|_2^2 = 0, \tag{4.12}$$

which comes from the fact that $\langle \mathbf{u}^{n+1}, \nabla_h (p^{n+1}-p^n)\rangle_1 = 0$. A combination of the last identity with (4.11) leads to

$$\begin{aligned} &E_h(\phi^{n+1}) - E_h(\phi^n) + \frac{1}{2\gamma}(\|\mathbf{u}^{n+1}\|_2^2 - \|\mathbf{u}^n\|_2^2) + \frac{\Delta t^2}{2\gamma}(\|\nabla_h p^{n+1}\|_2^2 - \|\nabla_h p^n\|_2^2) \\ &+ \frac{\nu\Delta t}{\gamma}\|\nabla_h \bar{\mathbf{u}}^{n+1}\|_2^2 + \Delta t\|\nabla_h \mu^{n+1}\|_2^2 \leq 0. \end{aligned} \tag{4.13}$$

This is exactly the inequality (4.2), so that the total energy dissipation rate is established. This finishes the proof of Theorem 4.1. □

Remark 4.1 For the phase field model coupled with fluid motion, there have been quite a few existing works of optimal rate convergence analysis and error estimate, such as the ones for the

Cahn-Hilliard-Hele-Shaw [3, 6, 39], Cahn-Hilliard-Navier-Stokes [10] flows, as well as the one [4] coupled with the Darcy flow. Due to the energy structure, the standard $\ell^\infty(0, T; \ell^2)$ error estimate does not work out directly; instead, the $\ell^\infty(0, T; H_h^1) \cap \ell^2(0, T; H_h^3)$ convergence estimate has to be applied, so that the nonlinear errors associated with the phase variable convective term could be cancelled. This technique has played a key role in the convergence analysis for the Cahn-Hilliard-fluid models.

Meanwhile, all these existing works have been based on a phase energy with a polynomial approximation. For the Cahn-Hilliard-Navier-Stokes system (1.2)–(1.4), with Flory-Huggins phase energy (1.1), an optimal rate convergence analysis for the proposed numerical scheme (2.20)–(2.23) is expected to be valid. In comparison with the analysis reported for the Cahn-Hilliard-fluid models with polynomial approximation phase energy, the essential difficulties are associated with the singular nature of the logarithmic terms. In turn, a uniform distance between the numerical solution and the singular limit value has to be established, locally in time, so that the convergence estimate could go through. Because of the nonlinear and singular nature of the logarithmic term, the technique of combining the rough and refined error estimates has to be applied in the convergence analysis; see the related works for the nonlocal Cahn-Hilliard equation [32, 33], porous medium equation [15, 16], Poisson-Nernst-Planck system [37], etc. The details will be presented in a future work.

Remark 4.2 For the Cahn-Hilliard-fluid model based on a phase energy with a polynomial approximation, there have been some existing works of second order numerical schemes [3, 10]. Meanwhile, for the pure phase field equation with logarithmic energy potential, a few second order numerical schemes have also been reported [5, 7, 14], based on either the Crank-Nicolson or backward differentiation formula (BDF) approach, in which both the positivity-preserving and energy stability properties have been analyzed at a theoretical level.

For the Cahn-Hilliard-Navier-Stokes system (1.2)–(1.4), with Flory-Huggins phase energy (1.1), a second order numerical scheme could be derived in a similar manner. A modified Crank-Nicolson approximation will be used as the temporal discretization, following the idea reported in [5]. Semi-implicit approximations will be applied in the nonlinear convective terms. The positivity-preserving and energy stability analyses are expected for this numerical scheme.The details will be presented in a future work.

Remark 4.3 For simplicity of presentation, we have taken a constant mobility, $\mathcal{M}(\phi) \equiv 1$, in Eq. (1.3). If a variable mobility is taken into consideration, i.e., if the mobility function is phase variable dependent, the numerical scheme (2.20)–(2.23) could be derived in the same fashion, and the positivity preserving and energy stability estimates could be established, following similar ideas presented in this paper. In particular, the operator $\mathcal{G}_h$ will be redefined, while a similar monotonicity analysis is available. Moreover, the discrete maximum norm bound of the inverse elliptic operator associated with the temporal derivative is needed, following the estimates derived in a few related works [7, 37]. All these modified estimates will lead to the desired results of both positivity preserving and energy stability properties. The technical details are left to interested readers.

5 Numerical Results

In this section we present some numerical results, using the proposed method (2.20)–(2.23). A preconditioned steepest descent (PSD) iteration algorithm is applied in the numerical implementation of (2.21); the theoretical foundation of the PSD iteration has been analyzed

in [20], and its application has been reported for various gradient flow models [8, 19, 21, 49], etc.

5.1 Convergence Test for the Numerical Scheme

In this subsection we verify the accuracy of the numerical scheme (2.20)–(2.23). The computational domain is chosen as $\Omega = (0, 1)^2$ for simplicity, and the exact solution of the phase variable, velocity field, and the pressure field are given by

$$\begin{aligned} \Phi &= \frac{1}{\pi}\sin(2\pi x)\cos(2\pi y)\cos(t), \\ \mathbf{u} &= \begin{pmatrix} -\cos(2\pi x)\sin(2\pi y)\cos(t) \\ \sin(2\pi x)\cos(2\pi y)\cos(t) \end{pmatrix}, \\ P &= \sin(2\pi x)\sin(t), \end{aligned}$$

and the equations are modified to include appropriate source terms in order to ensure that the exact solution presented above does solve the system exactly. We also modify our algorithm to accommodate these source terms in our numerics of course. Notice that the phase variable Φ stays between -1 and 1, so that no singularity occurs during computation. For our numerical experiment, we set the time size as $\triangle t = 8h^2$, so that spatial and temporal accuracy can be checked simultaneously as the scheme is formally first order in time and second order in space. The final time is chosen as $T = 1$. The surface diffusion parameter ε and the expansive parameter θ_0 are given by 0.5 and 3 respectively, while the kinematic viscosity ν and the surface tension parameter γ are both set to 1. A sequence of spatial resolution is chosen: $N = 48 : 16 : 256$. The expected temporal numerical accuracy assumption $e \approx C(\triangle t + h^2)$ indicates that $\ln|e| \approx \ln C - 2\ln N$, so that we plot $\ln|e|$ vs. $\ln N$ to demonstrate the convergence order. Specific numerical errors are displayed in Fig. 1. The slopes of the fitted lines related to three different physical variables are given by -2.0009, -2.0457 and -1.9495, respectively. This verifies the first order accuracy in time and second order accuracy in space.

5.2 Simulation of the Interface Pinchoff

In this subsection we report results on our simulation of binary fluids with topological interface changes. A similar experiment has been performed in [25, 27]. The computational domain is set as $(0, 1)^2$, and we assume that the density variance of two fluids is small so that a Boussinesq approximation can be used for simplicity. The following buoyancy term is added to the Navier-Stokes equation in (2.20):

$$-b(\phi)\hat{\mathbf{y}} = -G(\rho(\phi) - \bar{\rho})\hat{\mathbf{y}} = -G\frac{\rho_1 - \rho_2}{2}(\phi - \bar{\phi})\hat{\mathbf{y}} := -\lambda(\phi - \bar{\phi})\hat{\mathbf{y}},$$

where $\hat{\mathbf{y}}$ is the unit vector pointing upward $\big(\hat{\mathbf{y}} = (0, 1)\big)$, G is the gravitational constant, $\rho(\phi) = \frac{1+\phi}{2}\rho_1 + \frac{1-\phi}{2}\rho_2$, $\bar{\rho}$ is the spatially averaged density, $\bar{\phi}$ is the spatially averaged order parameter, and $\lambda = G\frac{\rho_1-\rho_2}{2}$. In addition, two interfaces that are small perturbations of flat ones are introduced:

$$y_1(x) = \frac{1}{2} - \frac{0.5 + 0.1\cos(x)}{2\pi}, \quad y_2(x) = \frac{1}{2} + \frac{0.5 + 0.1\cos(x)}{2\pi}, \tag{5.1}$$

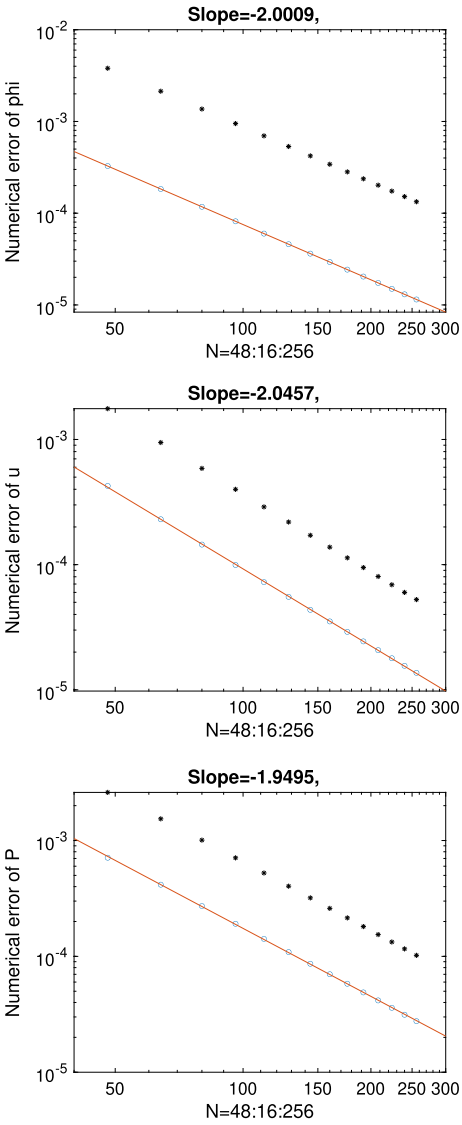

Fig. 1 The discrete ℓ^2 and ℓ^∞ numerical error vs. spatial resolution N for $N = 48 : 16 : 256$, and the time step size is set as $\triangle t = 8h^2$. The numerical results are obtained via numerical scheme (2.20)–(2.23). All the data shown in this figure lie roughly on curves CN^{-2}, which agrees with the theoretical analysis

and the initial condition for the phase variable is given by

$$\phi_0 = 0.8 \tanh\left(\frac{y - y_1(x)}{\sqrt{2}\epsilon}\right) \tanh\left(\frac{y - y_2(x)}{\sqrt{2}\epsilon}\right).$$

In this simulation, we take $\nu = 0.001, \gamma = 5, \theta_0 = 3.2, \epsilon = 0.01$, and $\rho_1 = 1, \rho_2 = 2$. The spatial mesh and time step size are taken as 1/256 and 1e-4, respectively. The snapshot plots of the physical variables are displayed in Fig. 2. It is observed that the patterns of these results are similar to the ones reported in [27].

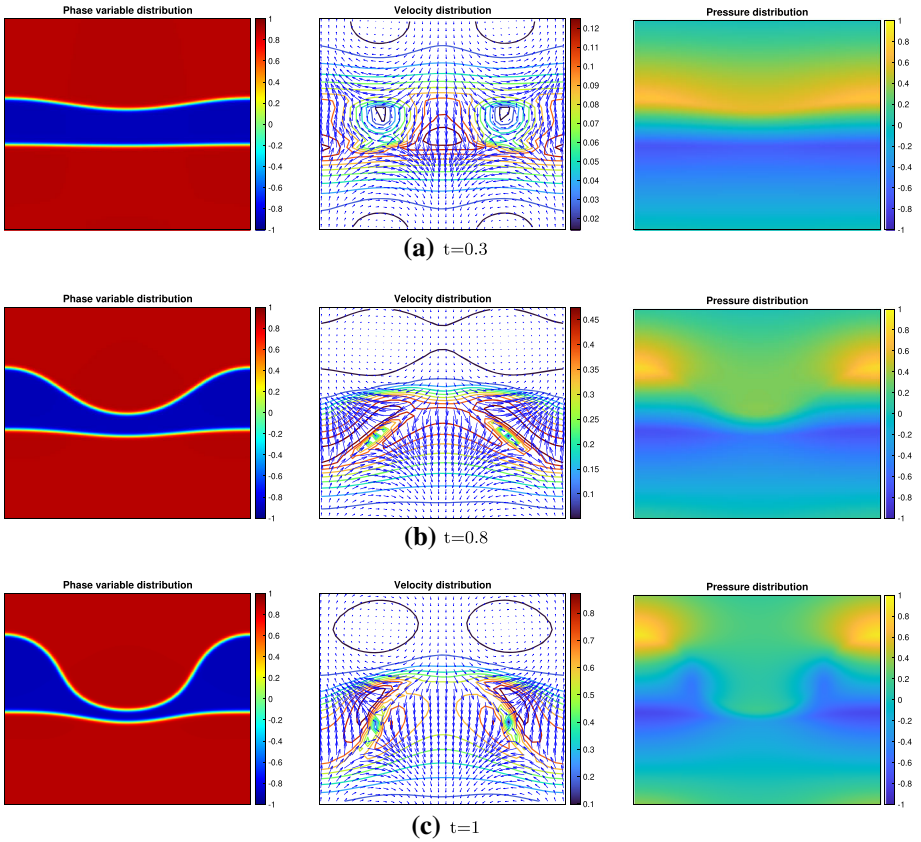

Fig. 2 Time snapshot plots of the interface pinchoff simulation. In each time snap we plot the phase variable, velocity field and pressure distribution, respectively. The parameters are given by $\nu = 0.001$, $\gamma = 5$, $\theta_0 = 3.2$, $\varepsilon = 0.01$, and $\rho_1 = 1$, $\rho_2 = 2$

5.3 Simulation with a Random Initial Data

To test the positivity-preserving property and energy stability, we give a two-dimensional numerical simulation over $\Omega = (0, 1)^2$. Here the parameters are set to be: $\theta_0 = 3.4$, $\epsilon = 0.005$, $\nu = 1$ and $\gamma = 2$. In this experiment we still take the time and spatial step size as $\Delta t = 1e - 4$ and $h = 1/256$. The initial value is given by

$$\phi_0 = 0.2 + 0.05(2r_{i,j} - 1), \quad \text{where } r_{i,j} \text{ are uniformly distributed random numbers in } [0, 1]. \tag{5.2}$$

Eight snapshot plots in the simulation are displayed in Fig. 3. At $t = 10$, a single structure emerges out of the random small scale initial data. Fig. 4 presents the time evolution of the minimum and maximum values of the phase variable. It is observed that the minimum value remains above -0.9303, while the maximum value remains 0.9185, so that the positivity preserving property (for both $1 + \phi$ and $1 - \phi$) has been verified in the numerical simulation. In addition, the energy evolution curve, displayed in Fig. 5, verifies the energy dissipation of the proposed numerical scheme.

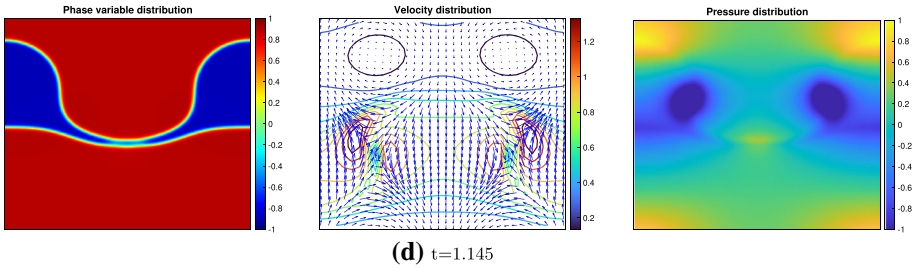

(d) t=1.145

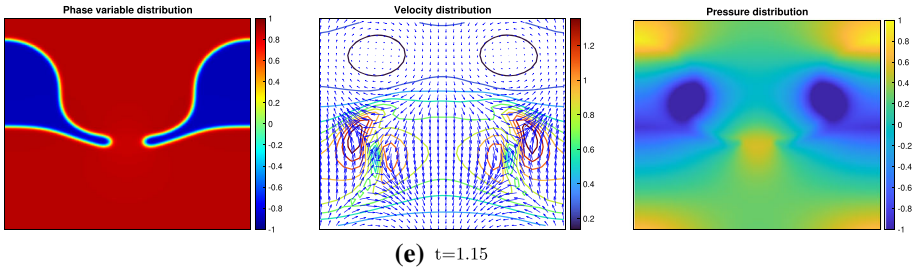

(e) t=1.15

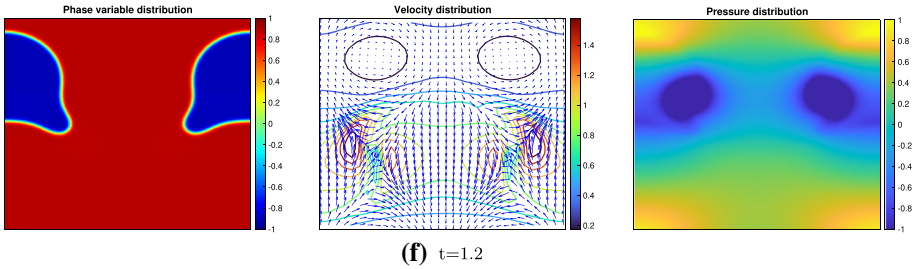

(f) t=1.2

Fig. 2 continued

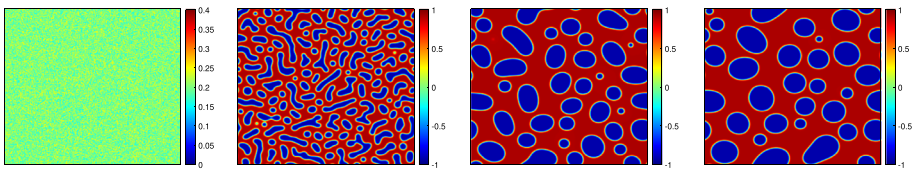

(a) t=0 **(b)** t=0.005 **(c)** t=0.05 **(d)** t=0.1

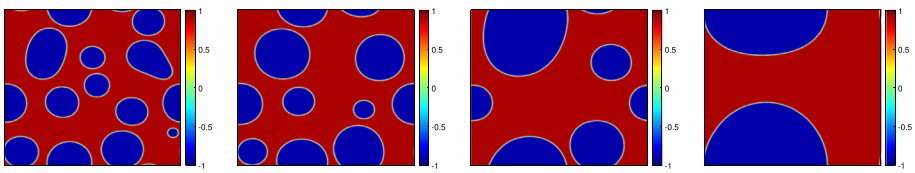

(e) t=0.5 **(f)** t=1 **(g)** t=3 **(h)** t=10

Fig. 3 Time snapshot plots captured during the simulation with the random initial condition (5.2). The phase variable begins to separate and form many small structures, and eventually merges to one single structure

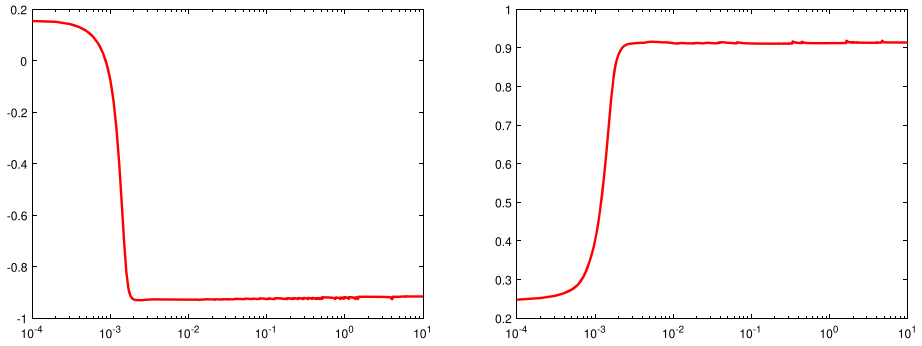

Fig. 4 The time evolution of minimum value (left) and maximum value (right) of the phase variable, with the random initial data (5.2)

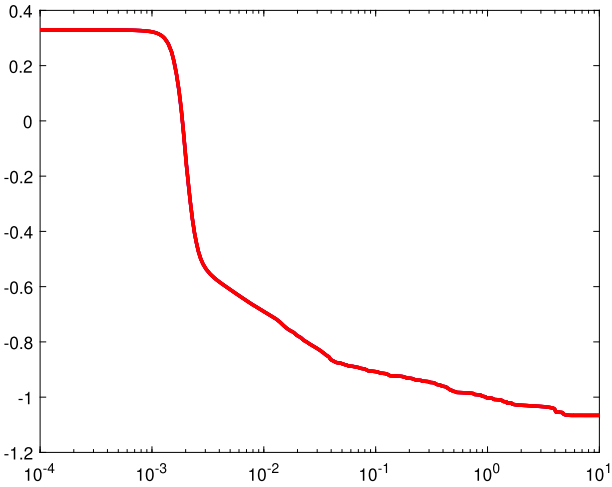

Fig. 5 Semilog plot of the energy evolution with the modified energy (4.2), with the random initial data (5.2)

6 Concluding Remarks

In this paper we have presented and analyzed a finite difference numerical scheme for the Cahn-Hilliard-Navier-Stokes system, with logarithmic Flory-Huggins energy potential. A convex splitting numerical approximation is applied to the singular chemical potential: implicit treatment for the logarithmic term and the surface diffusion term, combined with an explicit update for the linear expansive term. For the convective term in the phase field evolutionary equation, the phase variable is computed explicitly, while the velocity vector is treated implicitly. A similar semi-implicit algorithm is applied to the fluid momentum equation: implicit treatment for the kinematic diffusion term, explicit update for the pressure gradient, combined with semi-implicit approximations to the fluid convection and the phase field coupled term, respectively. In turn, this semi-implicit method generates an intermediate velocity field, and a Helmholtz projection into the divergence-free vector field yields the velocity vector and the pressure variable at the next time step. This decoupled approach avoids a complicated Stokes solver, and the numerical efficiency is greatly improved. In addition, we make use of the singular and convex nature of the logarithmic term, as well

as the monotonicity analysis of the velocity solver, and come up with a nonlinear iteration process to construct the numerical solution. With the help of careful estimates, the unique solvability and the positivity-preserving analysis (for the logarithmic arguments) could be theoretically established. The energy stability analysis has also been carefully derived, which indicates a dissipative total energy at a discrete level. Some numerical results are presented, which demonstrate the robustness and efficiency of the numerical scheme.

Acknowledgements This work is supported in part by the grants NSFC 12071090 (W. Chen), NSF DMS-2012269 (C. Wang), NSFC 11871159, Guangdong Provincial Key Laboratory for Computational Science and Material Design 2019B030301001 (X. Wang). C. Wang also thanks the Key Laboratory of Mathematics for Nonlinear Sciences, Fudan University, for the support.

Funding The authors have not disclosed any funding.

Data Availibility not applicable

Declarations

Conflict of interest not applicable

Code Availability not applicable

Ethics Approval not applicable

Consent to Participate not applicable

Consent for Publication not applicable

References

1. Browder, F.: Nonlinear elliptic boundary value problems. Bull. Amer. Math. Soc. **69**, 962–874 (1963)
2. Cahn, J.W., Elliott, C.M., Novick-Cohen, A.: The Cahn-Hilliard equation with a concentration dependent mobility: Motion by minus the Laplacian of the mean curvature. Europ. J. Appl. Math. **7**, 287–301 (1996)
3. Chen, W., Feng, W., Liu, Y., Wang, C., Wise, S.M.: A second order energy stable scheme for the Cahn-Hilliard-Hele-Shaw equation. Discrete Contin. Dyn. Syst. Ser. B **24**(1), 149–182 (2019)
4. Chen, W., Han, D., Wang, C., Wang, S., Wang, X., Zhang, Y.: Error estimate of a decoupled numerical scheme for the Cahn-Hilliard-Stokes-Darcy system. IMA J. Numer. Anal., (2022). accepted and published online: https://doi.org/10.1093/imanum/drab046
5. Chen, W., Jing, J., Wang, C., Wang, X., Wise, S.M.: A modified Crank-Nicolson scheme for the Flory-Huggin Cahn-Hilliard model. Commun. Comput. Phys. **31**(1), 60–93 (2022)
6. Chen, W., Liu, Y., Wang, C., Wise, S.M.: An optimal-rate convergence analysis of a fully discrete finite difference scheme for Cahn-Hilliard-Hele-Shaw equation. Math. Comp. **85**, 2231–2257 (2016)
7. Chen, W., Wang, C., Wang, X., Wise, S.M.: Positivity-preserving, energy stable numerical schemes for the Cahn-Hilliard equation with logarithmic potential. J. Comput. Phys.: X **3**, 100031 (2019)
8. Cheng, K., Wang, C., Wise, S.M.: An energy stable Fourier pseudo-spectral numerical scheme for the square phase field crystal equation. Commun. Comput. Phys. **26**, 1335–1364 (2019)
9. Copetti, M.I.M., Elliott, C.M.: Numerical analysis of the Cahn-Hilliard equation with a logarithmic free energy. Numer. Math. **63**, 39–65 (1992)
10. Diegel, A., Wang, C., Wang, X., Wise, S.M.: Convergence analysis and error estimates for a second order accurate finite element method for the Cahn-Hilliard-Navier-Stokes system. Numer. Math. **137**, 495–534 (2017)
11. Doi, M.: Soft Matter Physics. Oxford University Press, Oxford, UK (2013)
12. Dong, L., Wang, C., Wise, S.M., Zhang, Z.: A positivity-preserving, energy stable scheme for a ternary Cahn-Hilliard system with the singular interfacial parameters. J. Comput. Phys. **442**, 110451 (2021)

13. Dong, L., Wang, C., Zhang, H., Zhang, Z.: A positivity-preserving, energy stable and convergent numerical scheme for the Cahn-Hilliard equation with a Flory-Huggins-deGennes energy. Commun. Math. Sci. **17**, 921–939 (2019)
14. Dong, L., Wang, C., Zhang, H., Zhang, Z.: A positivity-preserving second-order BDF scheme for the Cahn-Hilliard equation with variable interfacial parameters. Commun. Comput. Phys. **28**, 967–998 (2020)
15. Duan, C., Chen, W., Liu, C., Wang, C., Yue, X.: A second order accurate, energy stable numerical scheme for one-dimensional porous medium equation by an energetic variational approach. Commun. Math. Sci., (2022). Accepted and in press
16. Duan, C., Liu, C., Wang, C., Yue, X.: Convergence analysis of a numerical scheme for the porous medium equation by an energetic variational approach. Numer. Math. Theor. Meth. Appl. **13**, 1–18 (2020)
17. E, W., Liu, J.-G.: Projection method III. Spatial discretization on the staggered grid. Math. Comp. **71**, 27–47 (2002)
18. Elliott, C.M., Garcke, H.: On the Cahn-Hilliard equation with degenerate mobility. SIAM J. Math. Anal. **27**, 404–423 (1996)
19. Feng, W., Guan, Z., Lowengrub, J.S., Wang, C., Wise, S.M., Chen, Y.: A uniquely solvable, energy stable numerical scheme for the functionalized Cahn-Hilliard equation and its convergence analysis. J. Sci. Comput. **76**(3), 1938–1967 (2018)
20. Feng, W., Salgado, A.J., Wang, C., Wise, S.M.: Preconditioned steepest descent methods for some nonlinear elliptic equations involving p-Laplacian terms. J. Comput. Phys. **334**, 45–67 (2017)
21. Feng, W., Wang, C., Wise, S.M., Zhang, Z.: A second-order energy stable Backward Differentiation Formula method for the epitaxial thin film equation with slope selection. Numer. Methods Partial Differential Equations **34**(6), 1975–2007 (2018)
22. Feng, X.: Fully discrete finite element approximations of the Navier-Stokes-Cahn-Hilliard diffuse interface model for two-phase fluid flows. SIAM J. Numer. Anal. **44**, 1049–1072 (2006)
23. Feng, X., Wise, S.M.: Analysis of a fully discrete finite element approximation of a Darcy-Cahn-Hilliard diffuse interface model for the Hele-Shaw flow. SIAM J. Numer. Anal. **50**, 1320–1343 (2012)
24. Guermond, J.L., Minev, P., Shen, J.: An overview of projection methods for incompressible flows. Comput. Methods Appl. Mech. Engrg. **195**, 6011–6045 (2006)
25. Han, D.: A decoupled unconditionally stable numerical scheme for the Cahn-Hilliard-Hele-Shaw system. J. Sci. Comput. **66**(3), 1102–1121 (2016)
26. Han, D., Wang, X.: A second order in time, uniquely solvable, unconditionally stable numerical scheme for Cahn-Hilliard-Navier-Stokes equation. J. Comput. Phys. **290**, 139–156 (2015)
27. Han, D., Wang, X.: Decoupled energy-law preserving numerical schemes for the Cahn-Hilliard-Darcy system. Numer. Methods Partial Differential Equations **32**(3), 936–954 (2016)
28. Harlow, F., Welch, J.: Numerical calculation of time-dependent viscous incompressible flow of fluid with free surface. Phys. Fluids **8**, 2182–2189 (1965)
29. Kay, D., Welford, R.: Efficient numerical solution of Cahn-Hilliard-Navier-Stokes fluids in 2D. SIAM J. Sci. Comput. **29**, 2241–2257 (2007)
30. Kim, J.S., Kang, K., Lowengrub, J.S.: Conservative multigrid methods for Cahn-Hilliard fluids. J. Comput. Phys. **193**, 511–543 (2003)
31. Li, D., Tang, T.: Stability of the semi-implicit method for the Cahn-Hilliard equation with logarithmic potentials. Ann. Appl. Math. **37**, 31–60 (2021)
32. Li, X., Qiao, Z., Wang, C.: Convergence analysis for a stabilized linear semi-implicit numerical scheme for the nonlocal Cahn-Hilliard equation. Math. Comp. **90**, 171–188 (2021)
33. Li, X., Qiao, Z., Wang, C.: Stabilization parameter analysis of a second order linear numerical scheme for the nonlocal Cahn-Hilliard equation. IMA J. Numer. Anal., (2022). Accepted and in press
34. Liu, C., Shen, J.: A phase field model for the mixture of two incompressible fluids and its approximation by a Fourier-spectral method. Physica D **179**, 211–228 (2003)
35. Liu, C., Shen, J., Yang, X.: Decoupled energy stable schemes for a phase-field model of two-phase incompressible flows with variable density. J. Sci. Comput. **62**(2), 601–622 (2015)
36. Liu, C., Wang, C., Wang, Y.: A structure-preserving, operator splitting scheme for reaction-diffusion equations with detailed balance. J. Comput. Phys. **436**, 110253 (2021)
37. Liu, C., Wang, C., Wise, S.M., Yue, X., Zhou, S.: A positivity-preserving, energy stable and convergent numerical scheme for the Poisson-Nernst-Planck system. Math. Comp. **90**, 2071–2106 (2021)
38. Liu, C., Wang, C., Wise, S.M., Yue, X., Zhou, S.: An iteration solver for the Poisson-Nernst-Planck system and its convergence analysis. J. Comput. Appl. Math. **406**, 114017 (2022)
39. Liu, Y., Chen, W., Wang, C., Wise, S.M.: Error analysis of a mixed finite element method for a Cahn-Hilliard-Hele-Shaw system. Numer. Math. **135**, 679–709 (2017)
40. Lowengrub, J.S., Truskinovsky, L.: Cahn-Hilliard fluids and topological transitions. Proc. R. Soc. Lond. A **454**, 2617–2654 (1998)

41. Minty, G.: On a monotonicity method for the solution of non-linear equations in Banach spaces. Proc. Nat. Acad. Sci. **50**, 1038–1041 (1963)
42. Qian, Y., Wang, C., Zhou, S.: A positive and energy stable numerical scheme for the Poisson-Nernst-Planck-Cahn-Hilliard equations with steric interactions. J. Comput. Phys. **426**, 109908 (2021)
43. Samelson, R., Temam, R., Wang, C., Wang, S.: Surface pressure Poisson equation formulation of the primitive equations: Numerical schemes. SIAM J. Numer. Anal. **41**, 1163–1194 (2003)
44. Samelson, R., Temam, R., Wang, C., Wang, S.: A fourth order numerical method for the planetary geostrophic equations with inviscid geostrophic balance. Numer. Math. **107**, 669–705 (2007)
45. Shen, J., Yang, X.: A phase-field model and its numerical approximation for two-phase incompressible flows with different densities and viscosities. SIAM J. Sci. Comput. **32**, 1159–1179 (2010)
46. Shen, J., Yang, X.: Decoupled, energy stable schemes for phase-field models of two-phase incompressible flows. SIAM J. Numer. Anal. **53**(1), 279–296 (2015)
47. Wang, C., Liu, J.-G.: Convergence of gauge method for incompressible flow. Math. Comp. **69**, 1385–1407 (2000)
48. Yuan, M., Chen, W., Wang, C., Wise, S.M., Zhang, Z.: An energy stable finite element scheme for the three-component Cahn-Hilliard-type model for macromolecular microsphere composite hydrogels. J. Sci. Comput. **87**, 78 (2021)
49. Zhang, J., Wang, C., Wise, S.M., Zhang, Z.: Structure-preserving, energy stable numerical schemes for a liquid thin film coarsening model. SIAM J. Sci. Comput. **43**(2), A1248–A1272 (2021)
50. Zhao, J.: A general framework to derive linear, decoupled and energy-stable schemes for reversible-irreversible thermodynamically consistent models. Comput. Math. Appl. **110**(5), 91–109 (2022)
51. Zhao, J., Han, D.: Second-order decoupled energy-stable schemes for Cahn-Hilliard-Navier-Stokes equations. J. Comput. Phys. **443**, 110536 (2021)
52. Zhao, J., Yang, X., Shen, J., Wang, Q.: A decoupled energy stable scheme for a hydrodynamic phase-field model of mixtures of nematic liquid crystals and viscous fluids. J. Comput. Phys. **305**, 539–556 (2016)